Nonlinear battery modeling using continuous-time system identification methods and non-uniformly sampled data

Markus Kneissl
Christian Doppler Laboratory for Innovative Control and Monitoring of Automotive Powertrain Systems
TU Wien
Vienna, Austria
markus.kneissl@tuwien.ac.at

Christoph Hametner
Christian Doppler Laboratory for Innovative Control and Monitoring of Automotive Powertrain Systems
TU Wien
Vienna, Austria
christoph.hametner@tuwien.ac.at

Markus Dohr
AVL List GmbH
Graz, Austria
markus.dohr@avl.com

***Abstract*—A battery model identification approach, based on non-uniformly sampled data, aiming to reflect the nonlinear dynamic behavior of a lithium-ion cell is presented in this work. To accurately predict the voltage response, the underlying model should reproduce the fast and slow dynamics of the battery cell. Therefore direct identification from non-uniformly sampled measurement data based on continuous-time model identification is applied. To take into account the nonlinear behavior of the battery, local linear model partitioning for the state of charge is performed. The resulting dynamic battery model is able to accurately predict the system response. With a parameter conversion to physically interpretable parameters, based on an equivalent circuit model, the parameter variance among similar cells and the temperature dependency of the model identification are investigated as well as the parameter characteristics over time. All results are based on non-uniformly sampled input output measurement data of three identical lithium-ion power cells.**

***Index Terms*—non-uniformly sampled data, continuous-time system identification, lithium-ion battery, aging data analysis**

I. Introduction

Lithium-ion batteries are the most promising technology in electric vehicles and serve as the steppingstone for future environmentally friendly mobility. Due to the high power and energy density of the lithium-ion cell [1], the battery management system needs to monitor the cell precisely to ensure a safe and reliable operation. Based on the measurements of the terminal voltage and the charge/discharge current, mathematical battery models are needed to compute estimations of the state of charge (SoC) and the state of health (SoH) of the battery cell [2].

One way of identifying battery models is by direct parameter estimation using an optimization algorithm [3], [4], [5], which estimates the unknown parameters of electro-thermal, physical and chemical models by minimizing an objective function. One of the widest used method for control oriented battery modeling is discrete-time system identification [6], [7] of empirical or equivalent circuit based models. Another approach is based on the electrochemical principles of the battery cell [8], which are described by coupled systems of partial differential equations. However, this is not suitable for system identification purposes, even though it describes the fundamental principles on which all other models are based. In this paper, a continuous-time approach based on the nonlinear modeling strategy of previous studies [6], [9] is applied. Continuous-time system identification can directly be used on non-uniformly sampled data and therefore circumvents problems related to choosing a sampling time. Such methods can also be applied for stiff systems and enable to accurately estimate time delay of non-integer multiples of the sampling time [10], [11].

In [12] an algorithm for continuous-time transfer function identification from non-uniformly sampled data is derived. This method enables the direct identification of continuous-time transfer functions by introducing an algebraic reformulation of the transfer function model. The continuous-time model parameters represent a linear relationship from the input to the output. To implement the nonlinear effects of the open circuit voltage (OCV) local linear models for several operating regions are computed. Based on a simple, user-defined partitioning, a local model network (LMN), see e.g. [6], using continuous-time local models is constructed. To enable physical interpretation of the identified model parameters and interpret the changes over the local linear models a conversion to equivalent circuit model (ECM) parameters is performed. With the new parameter set, the characteristics over the state of charge (SoC), the temperature dependency and the evolution of the parameters over the aging process can be evaluated on physical bases.

The remainder of this paper is divided into three sections. In Section II the battery model identification based on the non-uniformly sampled data is described in detail. In section III the equivalent circuit model conversion is derived, which enables the physical interpretation of the identified parameters. In the last section, Section IV, the simulation results are shortly discussed followed by a model parameter diversification study.

978-1-5386-4444-7/18/$31.00 ©2018 IEEE

The last part covers the evolution of the model parameter over the aging process of the battery cell.

II. Battery Model Identification

In this section, the battery model identification is derived. For the model identification, the inputs are the charge/discharge current and the SoC. The output is the terminal voltage of the cell. Based on measurement data, which is a non-uniformly sampled input output sequence, a method that can directly compute model parameters from the measurements is used. A sequence of the measurement data is shown in Fig. 1, where the voltage u and the SoC response to a step in the current i is depicted. In Fig. 2, the relative frequency

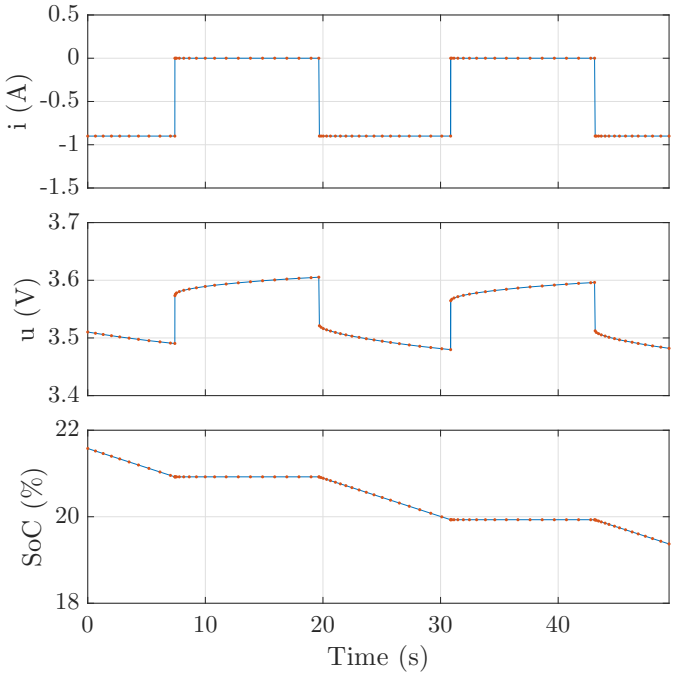

Fig. 1. Section of the measurement data of an input step and the corresponding voltage and SoC response clearly showing the non-uniform inter sampling behavior. Top: the input signal, middle: the voltage response and bottom: the SoC.

of the sampling intervals for one test cycle is depicted. The sampling intervals range from 0.1 ms up to 30 s and the most frequent sampling intervals are shown in the figure.

The rest of this section covers the continuous parameter estimation in detail, as well as the method used for the nonlinear model estimation.

A. Continuous-time model identification

Typically, the nonlinear dynamics of the battery cell are determined by the nonlinear effect of the SoC on the OCV. In [6] it is shown that local linear models are able to capture these effects in an efficient way. With the scheduling variable SoC, the operating regions of the local linear models are determined by simple user defined partitioning. For a more general approach the method described in [6] might be better suited.

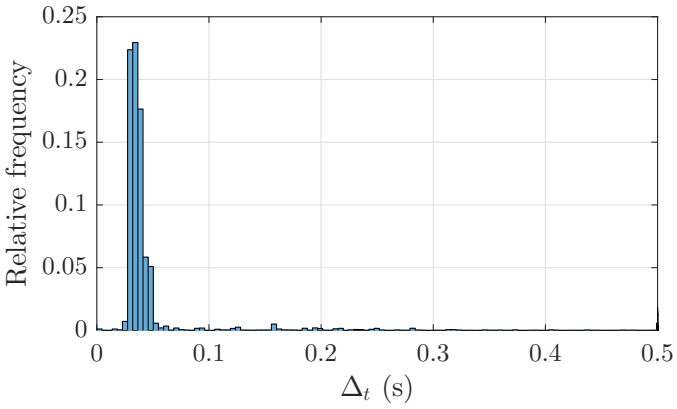

Fig. 2. Distribution of sampling intervals for a test cycle.

The local linear models are based on the linear differential equation

$$\begin{aligned}\ddot{y}(t) + a_1\dot{y}(t) + a_2 y(t) =& b_0\ddot{u}_1(t) + b_1\dot{u}_1(t) + b_2 u_1(t) \\ &+ cu_2(t) + du_3(t)\end{aligned} \tag{1}$$

which is the continuous-time equivalent of the discrete-time model used in [6]. The input signals are the applied current u_1, the SoC u_2 and the bias term u_3 which represents the affine term of the model. The corresponding transfer operator models are defined as follows

$$G_1(p) = \frac{b_0 p^2 + b_1 p + b_2}{p^2 + a_1 p + a_2} \tag{2}$$

$$G_2(p) = \frac{c}{p^2 + a_1 p + a_2} \tag{3}$$

$$G_3(p) = \frac{d}{p^2 + a_1 p + a_2} \tag{4}$$

with the argument p as the differential operator $p = \mathrm{d}/\mathrm{d}t$. As stated in [12] the isomorphism of the differential operator and the transfer function is valid and therefore the argument p corresponds to the transfer function description, i.e. the Laplace variable s. The transfer operator G_1 reflects the current response of the model and the influence of the SoC is given by G_2 and G_3. The unknown coefficients a_i, b_i, c and d have to be estimated. The algorithm for continuous-time model identification, shown in [12], for a given transfer operator

$$G(p) = \frac{B(p)}{A(p)} \tag{5}$$

where A and B fit the desired transfer operators (2)-(4) can be written in a general form as

$$G_0(p) = \frac{b_0 p^m + \ldots + b_m}{p^n + a_1 p^{n-1} + \ldots + a_n} \tag{6}$$

with m and n the corresponding highest derivatives. The method replaces the differential operator with a linear filter

$$\lambda = \frac{1}{1 + \tau p} \tag{7}$$

while keeping an exact transfer function. The filter parameter τ represents a tuning parameter, which has to be chosen

adequately. With that filter the following transformation can be made

$$G_0(p) = \frac{B(p)}{A(p)} = \frac{B^*(\lambda)}{A^*(\lambda)} = G_0^*(\lambda) \tag{8}$$

where A^* and B^* depend on the filter operator λ and the new parameters α and β in the following manner

$$A^*(\lambda) = 1 + \alpha_1\lambda + \alpha_2\lambda^2 + \cdots + \alpha_n\lambda^n \tag{9}$$
$$B^*(\lambda) = \beta_0 + \beta_1\lambda + \beta_2\lambda^2 + \cdots + \beta_m\lambda^m. \tag{10}$$

The transformation applied to the three transfer operators (2)-(4) and rewritten as input-output equation in regression form results in

$$\begin{aligned} y(t) = &- \alpha_1[\lambda y](t) - \alpha_2[\lambda^2 y](t) \\ &+ \beta_0 u_1(t) + \beta_1[\lambda u_1](t) + \beta_2[\lambda^2 u_1](t) \\ &+ \gamma[\lambda^2 u_2](t) + \delta[\lambda^2 u_3](t) \end{aligned} \tag{11}$$

where the direct influence of the input on the output is shown with the input $u_1(t)$. The filtered input and output signals are represented by $[\lambda u]$ and $[\lambda y]$. This equation is a dynamic system description valid at all points in time. Reformulation of (11) in matrix form yields

$$y(t) = \varphi_\tau^T(t)\theta_\tau \tag{12}$$

with the parameter vector

$$\theta_\tau = [\alpha_1 \quad \alpha_2 \quad \beta_0 \quad \beta_1 \quad \beta_2 \quad \gamma \quad \delta]^T \tag{13}$$

and the regressor vector

$$\begin{aligned} \varphi_\tau(t) = [&- [\lambda y](t), -[\lambda^2 y](t), \\ &u_1(t), [\lambda u_1](t), [\lambda^2 u_1](t), \\ &[\lambda^2 u_2](t), [\lambda^2 u_3](t)]^T \end{aligned} \tag{14}$$

For each of the local linear models of the LMN, the local parameter vector can now be estimated using weighted least squares (WLS). Each local model is valid for a small section of the SoC and the partitioning is chosen manually depending on the available training data. The weighting matrix W for the individual local models is obtained using Gaussian validity functions defined by its associated center and spread. The WLS estimator of the parameters (13) is given by

$$\theta_\tau = (\Phi_\tau^T W \Phi_\tau)^{-1} \Phi_\tau^T W Y \tag{15}$$

with Φ_τ the regressor matrix and Y the output vector defined as

$$\Phi_\tau = \begin{bmatrix} \varphi_\tau^T(t_1) \\ \varphi_\tau^T(t_2) \\ \vdots \\ \varphi_\tau^T(t_n) \end{bmatrix} \quad Y = \begin{bmatrix} y(t_1) \\ y(t_2) \\ \vdots \\ y(t_n) \end{bmatrix} \tag{16}$$

with t_1 to t_n representing the non uniformly distributed sampling instances.

With the parameter vector (15) and the desired parameter vector, comprising the unknown parameters from the transfer operator (2)-(4),

$$\theta = [a_1 \quad a_2 \quad b_0 \quad b_1 \quad b_2 \quad c \quad d]^T \tag{17}$$

the parameter transformation can be derived. The foundation of this transformation is formulated in [12] and the modified version, which fits the given system description, is stated here. The transformation is given by

$$\theta_\tau = F_\tau\theta + G_\tau \tag{18}$$

where

$$F_\tau = \begin{bmatrix} M_k & 0 & 0 & 0 \\ 0 & M_l & 0 & 0 \\ 0 & 0 & M_p & 0 \\ 0 & 0 & 0 & M_q \end{bmatrix} \tag{19}$$

is a $\Omega \times \Omega$ matrix with $\Omega = k + l + p + q$ and

$$k = n, \quad l = m + 1, \quad p = 1 \quad \text{and} \quad q = 1$$

representing the number of unknown parameters for a_i, b_i, c and d, respectively. The diagonal elements of (19) consist of Pascal matrices

$$M_\alpha = \begin{bmatrix} m_{11} & 0 & \cdots & 0 \\ \vdots & \ddots & \ddots & \vdots \\ \vdots & \ddots & \ddots & 0 \\ m_{\alpha 1} & \cdots & \cdots & m_{\alpha\alpha} \end{bmatrix} \tag{20}$$

which, depending on the position, are different in size, e.g. M_k a $k \times k$ square matrix, with their corresponding elements

$$m_{ij} = (-1)^{i-j} \binom{c-j}{i-j} \tau^{j+\Delta_\alpha} \tag{21}$$

with Δ_α the relative difference of the parameter, i.e. $\Delta_\alpha = k - \alpha, \quad \alpha \in \{k, l, p, q\}$. The second term in (18), G_τ is a $\Omega \times 1$ vector

$$G_\tau = [g_1 \cdots g_k \quad 0_{\Gamma\times 1}]^T \tag{22}$$

with $\Gamma = l + p + q$ and

$$g_i = \binom{k}{i} (-1)^i. \tag{23}$$

Now the transformation from (18) can be solved for the original parameter vector resulting in

$$\theta = F_\tau^{-1}(\theta_\tau - G_\tau). \tag{24}$$

The inverse of F can be computed if M is invertible, which is feasible for all values of $\tau > 0$.

III. Equivalent circuit model conversion

To enable physical interpretation of the identified model parameters and interpret the changes over the local linear models, a conversion from the transfer operator (2) to an ECM is derived in this section. For an arbitrary transfer function the foster synthesis, described in [13], can be applied which decomposes rational transfer functions to a series of RLC circuits. For the 2nd order ECM used in this paper the conversion, also shown in [14], is briefly described in this section.

The 2nd order ECM depicted in Fig. 3 consists of two RC elements in series and an ohmic resistor as well as a

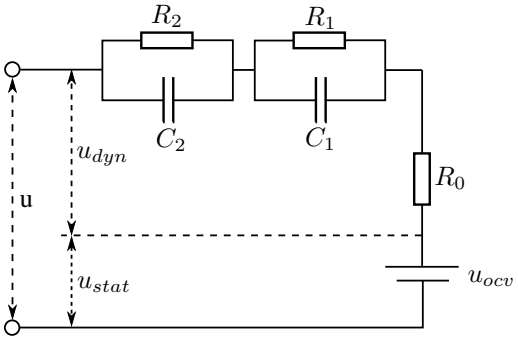

Fig. 3. Electric circuit of an ECM with two RC-elements.

constant voltage supply dependent on the OCV. This ECM is chosen as it fits the previous model order specification [6] and fortunately, as stated in [15], this is the best choice for an ECM. The dynamic part, u_{dyn} of the ECM can be described as

$$G_{ECM}(s) = R_0 + \frac{R_1}{1 + R_1 C_1 s} + \frac{R_2}{1 + R_2 C_2 s} \tag{25}$$

which enables the parameter conversion to the transfer function parameters of (2) and results in

$$\begin{aligned} b_0 &= R_0 \\ b_1 &= R_0(\frac{1}{\tau_1} + \frac{1}{\tau_2}) + \frac{1}{C_1} + \frac{1}{C_2} \\ b_2 &= \frac{R_0 + R_1 + R_2}{\tau_1 \tau_2} \\ a_1 &= \frac{1}{\tau_1} + \frac{1}{\tau_2} \\ a_2 &= \frac{1}{\tau_1 \tau_2} \end{aligned} \tag{26}$$

where $\tau_1 = R_1 C_1$ and $\tau_2 = R_2 C_2$ are the time constants of the dynamic system.

IV. Results

Three lithium-ion battery cells, which are aged over a period of 450 days, are used to validate the results of the continuous-time model identification. The investigated cells are 18650 Cells with Lithium Nickel Manganese Cobalt Oxide (NMC) as the Cathode material.

The used measurement data is divided in two parts, the reference test cycles (RTC) and the load cycles (LC). At the beginning of the aging test, five RTC are performed at different temperatures, which are used for initial model characterization. For the rest of the test alternating RTC at 25°C and LC at different loading conditions are performed. The conditions for the LC cover different amounts of cumulative ampere-hour throughput, various temperature levels, C-rates and depth of discharge. A measurement data set of a single RTC is depicted in Fig. 4. The applied current is shown in the first plot and the resulting voltage signal in the second plot. In the third plot the SoC is shown which is obtained through Coulomb counting. The data covers a large range of the SoC, with

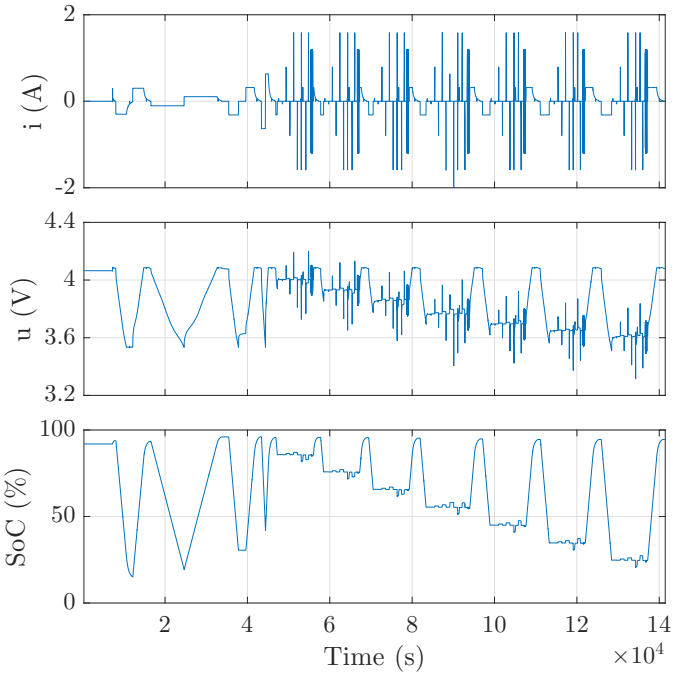

Fig. 4. Measurement data of a single reference test cycle.

complete charge and discharging cycles and highly dynamic current cycles at different SoC levels, which incorporate the fast and slow dynamics of the system.

A. Nonlinear model parameter and simulation results

The results of the simulation of an RTC at 25°C compared to the measurements is shown in Fig. 5. In the second plot the deviation between the two signals is depicted. The simulation results are computed with the training data since no validation data is available. However, since the identification was based on minimizing the one-step-ahead prediction error, these simulation results indicate that good generalization capabilities of the identified model can be expected.

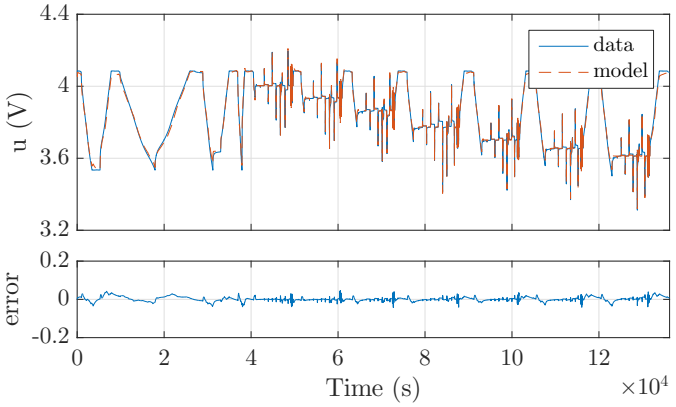

Fig. 5. Simulation result for a single reference test cycle and the corresponding error.

As mentioned before, at the beginning of the aging test five initial RTC are performed at various temperature levels

for all three cells. This RTCs are used for initial model characterization over a large temperature range. The internal resistance curve, i.e. $R_0/R_{0,init}$, versus the SoC of the non-linear identified models for each of the test cycles is shown on the left in Fig. 6. Here, the values are normalized using the initial internal resistance $R_{0,\,init}$ of Cell 1 at 25°C. By computing the mean value of each of this normalized curves the resulting values show the temperature dependency of the parameter $\bar{R}_0$, which are depicted on the right in Fig. 6. Each line on the left is projected to a single value on the right, to visualize the decrease of the internal resistance $\bar{R}_0$ with increasing temperature.

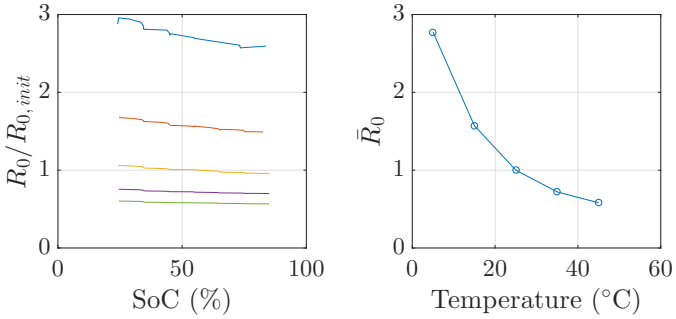

Fig. 6. Nonlinear values of the internal resistance R_0 versus the SoC for different temperature levels (left) and the mean value for each line versus corresponding temperatures (right).

B. Parameter distribution among new battery cells

To investigate the parameter characteristic among similar cells at the beginning of the life-cycle three similar cells are evaluated. All values depicted in this section are mean values of the nonlinear parameter characteristic over the SoC. Please note that all parameter values in Section IV-B and IV-C were normalized using the corresponding value of Cell 1 at 25°C. Each point is the result of a model identification from a RTC at various temperature levels. In Fig. 7 the mean normalized internal resistance $\bar{R}_0$ is depicted over the temperature for all three cells. As before the value decreases with increasing temperatures and for lower temperatures a slight variation in the parameters is visible. This effect is shown throughout the results and might be an indicator that the model identification is not as accurate for lower temperatures.

In Fig. 8 the parameters of the first RC-element, the slow time constant, is depicted. As observed in the internal resistance $\bar{R}_0$, a decrease of the resistance value $\bar{R}_1$ with increasing temperature is visible. The opposite effect is present in the temperature characteristics of the capacitance $\bar{C}_1$.

For the second RC-element, the same effect as for the other resistance values is visible where the resistance $\bar{R}_2$ decreases with increasing temperature. However, the parameter estimation for 5°C is significantly different from the other values and shows large deviations among the cells. The capacitance $\bar{C}_2$ on the other hand shows no deviation for the lowest temperature and an overall increase over the whole temperature range simular to $\bar{R}_1$.

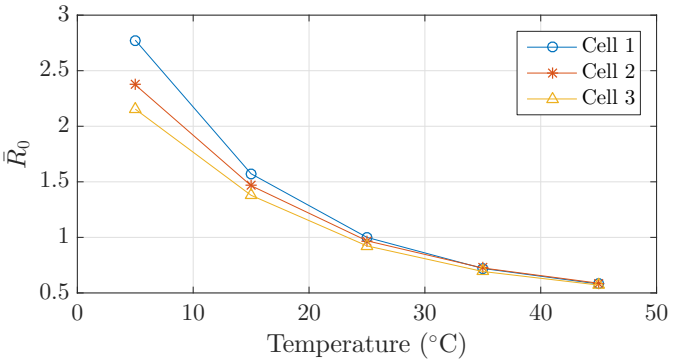

Fig. 7. Comparison of the internal resistance among similar unaged cells for different temperature levels.

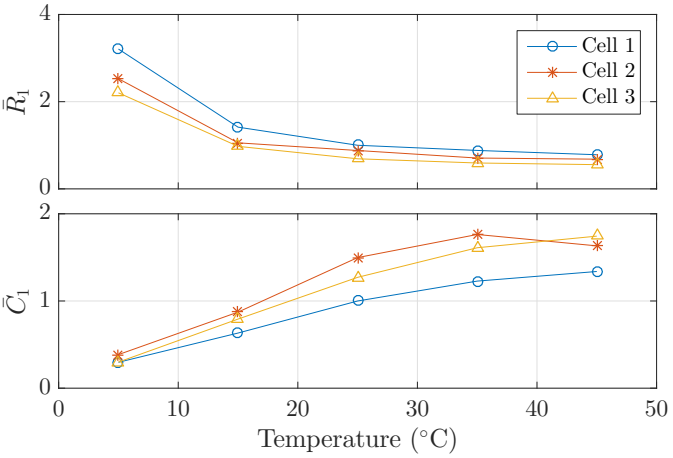

Fig. 8. Comparison of the first RC-element parameters among similar unaged cells for different temperature levels.

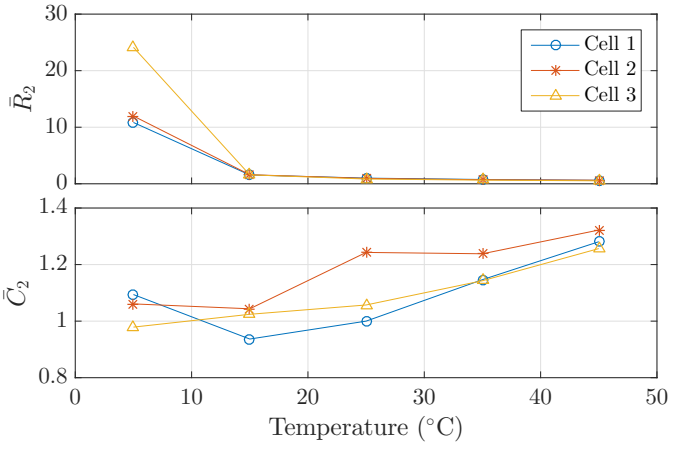

Fig. 9. Comparison of the second RC-element parameters among similar unaged cells for different temperature levels.

The results correspond with the findings in [16], which are based on experimental investigations of the temperature and aging effects of lithium-ion batteries at various conditions.

C. Parameter characteristics over the aging process

Additionally to the temperature dependent initial test cycles, extensive aging investigations have been performed for this cells. As mentioned before, the cells are aged under different conditions and normalized to the corresponding initial parameter value of Cell 1 at 25°C. Over the whole aging process, intermediate RTC at 25°C are performed. These intermediate tests, at the same temperature, are used for model investigation over the aging process and evaluation of the characteristic developments of the ECM parameters. As the capacity of the cell is one of the characteristic properties, the evolution of C_{act}/C_{nom} over the aging process is shown in Fig. 10. Here, C_{nom} refers to the the nominal capacity and the resulting normalized values show an almost constant decrease over the lifetime of the cell. The deviations among the cells are caused by the different test conditions at which the load cycles are performed.

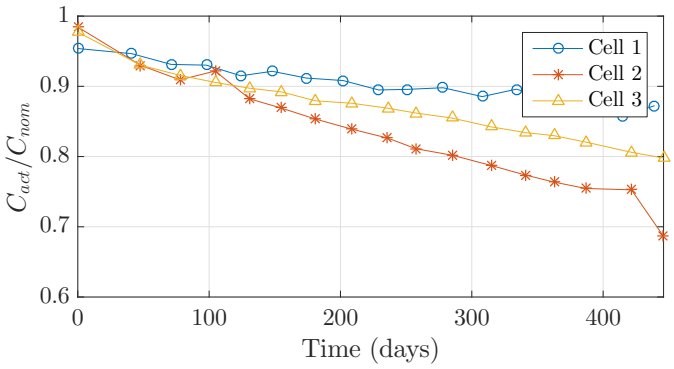

Fig. 10. Capacity decay of three cells at different stages of the aging process.

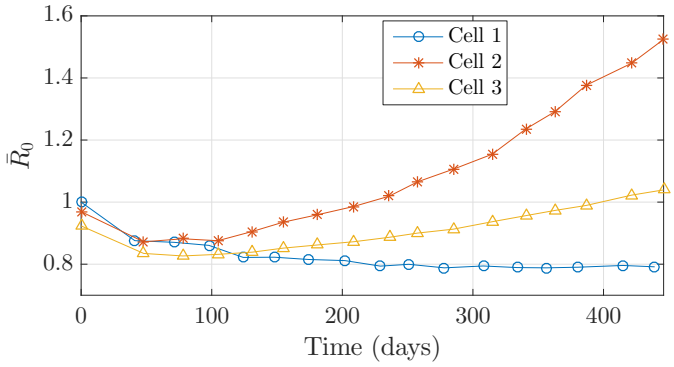

Fig. 11. Internal resistance progression of three cells at different stages of the aging process.

The evolution of the internal resistance for the intermediate RTC is shown in Fig. 11. The initial change in the parameters shows a decrease which is similar for all cells. From there on the characteristics deviate depending on the LC. The internal resistance $\bar{R}_0$ of Cell 1 continues to decrease up to 250 days and stays constant for the rest of the test period. The internal resistance of Cell 2 and 3 increase over the rest of the aging tests whereas the increase of Cell 2 is significantly larger.

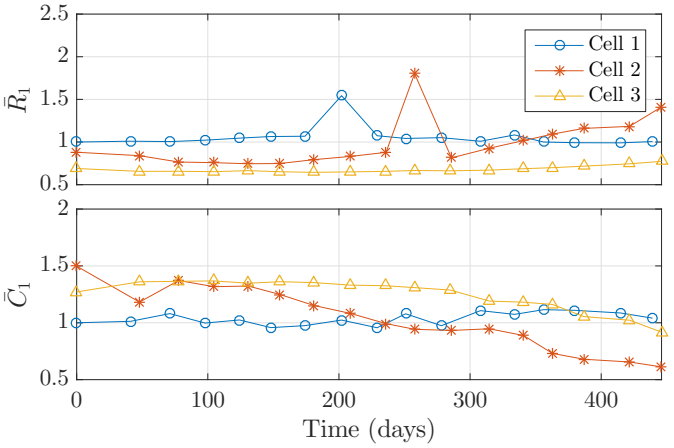

Fig. 12. Parameters of the first RC-element at different stages of the aging process.

For the parameters of the first RC-element, see Fig. 12, the deviations are not as significant as for the internal resistance. The resistance $\bar{R}_1$ of Cell 2 increases slightly and the capacitance $\bar{C}_1$ of both Cell 2 and Cell 3 decreases. For the rest of the cell parameters no significant changes are visible.

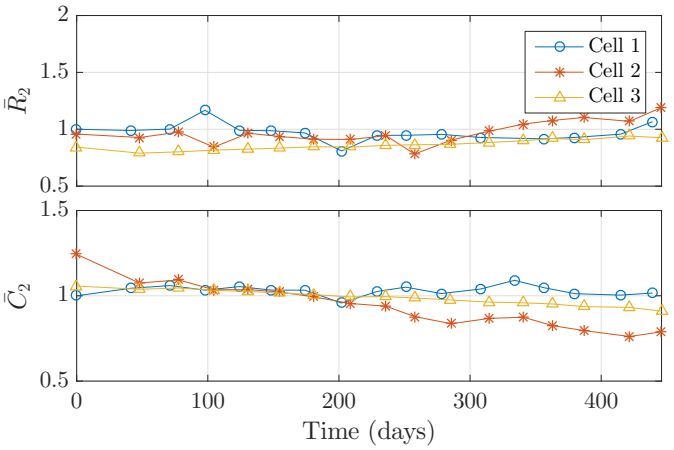

Fig. 13. Parameters of the second RC-element at different stages of the aging process.

For the second RC-element, shown in Fig. 13, the changes are similar to the result of the first RC-element.

Overall, the results show that all parameters change over time, but are highly dependent on the load history as shown in the capacity and internal resistance plot. The time constants on the other hand change rather slowly, as only for the most degraded cell marginal changes are visible.

V. Conclusion

The method described in this paper shows the accuracy and advantage of direct continuous-time model identification based

on non-uniformly sampled lithium-ion battery measurement data. The identified model is able to accurately predict the system response and with the ECM a physical interpretation of the parameters is possible. The effects of the parameters on the temperature and their characteristics over the aging of the cell are available without any data manipulation and solely based on direct identification. The results show the need of accurate estimation of the capacity and the internal resistance of the cell, as they are highly dependent on the load history. The changes of the other parameters are not as significant but will affect the model accuracy if not take into account. The future work goals are first of all the implementation of a SoC observer, to directly enable the use of measurement data without prior SoC calculation and the implementation of a SoH observer to adjust model parameters dependent on the changes in the capacity and the internal resistance.

ACKNOWLEDGMENT

The financial support by the Austrian Federal Ministry for Digital and Economic Affairs and the National Foundation for Research Technology and Development is gratefully acknowledged.

REFERENCES

[1] J.M. Tarascon, M. Armand, Issues and Challenges Facing Rechargeable Lithium Batteries. Nature, Volume 414, 2001, Pages 359-67.

[2] D. Andrea, Battery Management Systems for Large Lithium-Ion Battery Packs. Artech House, 2010.

[3] Y. Hu, S. Yurkovich, Y. Guezennec, B.J. Yurkovich, Electro-thermal battery model identification for automotive applications, Journal of Power Sources, Volume 196, Issue 1, 2011, Pages 449-457.

[4] K. Thirugnanam, E. R. J. T. P., M. Singh, P. Kumar, Mathematical Modeling of Li-Ion Battery Using Genetic Algorithm Approach for V2G Applications, IEEE Transactions on Energy Conversion, Volume 29, Issue 2, June 2014, Pages 332-343.

[5] L. Zhang, L. Wang, G. Hinds, C. Lyu, J. Zheng, J. Li, Multi-objective optimization of lithium-ion battery model using genetic algorithm approach, Journal of Power Sources, Volume 270, 2014, Pages 367-378, https://doi.org/10.1016/j.jpowsour.2014.07.110.

[6] C. Hametner, S. Jakubek, State of charge estimation for lithium ion cells: Design of experiments, nonlinear identification and fuzzy observer design, Journal of Power Sources, Volume 238, 2013, Pages 413-421.

[7] H. He, X. Zhang, R. Xiong, Y. Xu, H. Guo, Online model-based estimation of state-of-charge and open-circuit voltage of lithium-ion batteries in electric vehicles, Energy, Volume 39, Issue 1, 2012, Pages 310-318, https://doi.org/10.1016/j.energy.2012.01.009.

[8] S. Tang, L. Camacho-Solorio, Y. Wang, M. Krstic, State-of-Charge estimation from a thermalelectrochemical model of lithium-ion batteries, Automatica, Volume 83, 2017, Pages 206-219, https://doi.org/10.1016/j.automatica.2017.06.030.

[9] C. Hametner, W. Prochazka, A. Suljanovic and S. Jakubek, Model based Lithium Ion cell ageing data analysis, 2014 IEEE International Conference on Fuzzy Systems (FUZZ-IEEE), Beijing, 2014, Pages 962-967, https://doi.org/10.1109/FUZZ-IEEE.2014.6891641

[10] H. Unbehauen, G.P. Rao, Continuous-time approaches to system identificationA survey, Automatica, Volume 26, Issue 1, 1990, Pages 23-35, https://doi.org/10.1016/0005-1098(90)90155-B.

[11] H. Garnier, P.C. Young, What does continuous-time model identification have to offer?, IFAC Proceedings Volumes, Volume 45, Issue 16, 2012, Pages 810-815, https://doi.org/10.3182/20120711-3-BE-2027.00233.

[12] R. Johansson, Continuous-time model identification and state estimation using non-uniformly sampled data, IFAC Proceedings, Volumes 42, Issue 10, 2009,Pages 1163-1168.

[13] R. Ionutiu,R. Joost, A framework for synthesis of reduced order models, COMSON Handbook, 2009.

[14] B. Xia, et al, Accurate Lithium-ion battery parameter estimation with continuous-time system identification methods, Applied energy, Volume 179, 2016, Pages 426-436.

[15] S. Nejad, D.T. Gladwin, D.A. Stone, A systematic review of lumped-parameter equivalent circuit models for real-time estimation of lithium-ion battery states, Journal of Power Sources, Volume 316, 2016, Pages 183-196.

[16] W. Waag, S. Kbitz, D.U. Sauer, Experimental investigation of the lithium-ion battery impedance characteristic at various conditions and aging states and its influence on the application, Applied Energy, Volume 102, 2013, Pages 885-897, https://doi.org/10.1016/j.apenergy.2012.09.030